Numerical simulation of the unsteady flow past a cavity and application to the sunroof buffeting*

Denis Ricot†, Virginie Maillard‡ and Christophe Bailly§

†, ‡ Direction de la Recherche, Renault S.A.
TCR RUC 4 05, 1 avenue du golf
78288 Guyancourt cedex, France.

§ Laboratoire de Mécanique des Fluides et d'Acoustique
Ecole Centrale de Lyon & UMR CNRS 5509
BP 163, 69131 Ecully cedex, France.

Abstract

Coupling between vortex shedding over automotive sunroof and acoustic resonance of the passenger compartment can induce strong self-sustained oscillations of the flow. The maximum amplitude oscillation occurs when the frequency of an aerodynamic instability matches the resonance frequency of the vehicle. A detailed study of the phenomenon shows that aerodynamic coupling also participates to the self-sustained oscillation when the flow characteristics lead to aerodynamic frequencies outside the "matching frequency range". For the numerical prediction of the sunroof buffeting, both coupling mechanisms have to be computed. A CFD solver based on Lattice Boltzmann Method has been tested on simple bidimensional cases and the results have been compared to experimental data. Although a frequency shift of the successive stages of oscillation is observed, the simulation of the aerodynamic feedback loop is achieved. The deviation from experimental measurements is mainly due to the damping influence of the eddy viscosity model. The propagation of a pressure pulse and the acoustic response of a Helmholtz-like cavity have been simulated. The results show very good agreement with theory and numerical simulation performed with Boundary Element Method. Finally, the response of the bidimensional Helmholtz-like cavity under grazing flow has been investigated. Maximum amplitude of oscillation and frequency lock-on are observed at the frequency matching. The acoustic coupling is predicted by the LBM solver.

†PhD student

‡Research Engineer, Renault S.A.

§Assistant Professor, Member AIAA

1. Introduction

In automotive industry, aerodynamically induced noise represents a significant contributor to noise pollution inside passenger compartment. Flow-excited cavity is one of phenomena particularly efficient in the generation of aeroacoustic sources. Tonal cavity noise can be created by two different mechanisms.

First, at high Reynolds numbers, the incoming boundary layer is turbulent. So, stochastic fluctuations of flow over the cavity can excite the opening with a broadband spectrum. Inside and outside the cavity, emergent frequencies corresponding to cavity resonance frequencies can be found in acoustic pressure spectra. Tonal noise from car door cavities is a good example of this kind of discrete sound generation. The main feature of this mechanism is that the emergent frequencies do not depend on the grazing flow velocity but depend only on the geometry of the system.

When the ratio between the length L of the opening and the boundary layer thickness δ_0 of the grazing flow is large enough, aerodynamic instabilities can grow in the shear layer. Aerodynamic feedback or/and acoustic coupling lead to a coherent organization of flow instabilities. This is the second mechanism for the generation of discrete sound : emergent frequencies result from the periodic organization of the flow over the cavity. The problem of

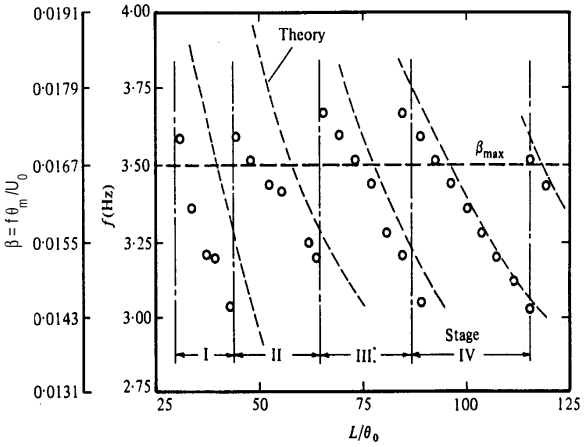

Figure 1: Experimental study of the sheartone (Ziada[29]). Strouhal number $\beta = f\theta_m/U_0$ of mixing-layer-wedge oscillation as a function of impingement length L.

the flow buffeting over automotive sunroof belongs to this kind of flow-excited cavity. Empirical value of $L/\delta_0 \approx 3-5$ for the limit of possible periodic oscillations of flow is found[26,30] and in the rest of this paper we shall suppose that the boundary layer thickness/opening ratio is larger than this threshold and we shall deal only with the mechanism of tonal noise generation involving periodically shedding of aerodynamic disturbances.

1.1 Physics of the sheartone

The cavity tone problem has been studied extensively over the past four decades. Most of the first studies were conducted at flow velocity near and above Mach numbers of one, with applications to aeronautics. Some models for the prediction of oscillation frequencies have been developed[2,25,27] on the idea that the periodic nature of shear layer instabilities is the result of the upstream influence of the acoustic source produced by the impingement of vorticity fluctuations upon the downstream edge. Even if some authors[27] account for acoustic reflections on neighbouring solid walls, the self-sustained oscillation of the flow is independent of the presence of a cavity. The phenomenon is often called sheartone by analogy with the jet-tone or edgetone (self-sustained oscillation of a jet impinging an edge). If the impingement length L is much smaller than the acoustic wavelength λ_a, the sensitive region of the shear layer lies in the nonpropagating pressure field (pseudosound region). For example, it happens for experiments conducted at very low Mach number,[5,16,29,30] and of course for numerical simulations performed with an incompressible CFD solver.[10,22] In these cases, the self-sustained oscillation mechanism can be considered as purely aerodynamic. The frequency of the incompressible sheartone can be estimated by the relation[23]

$$f \approx n\frac{U_c}{L} \tag{1}$$

where U_c is the convection velocity of aerodynamic disturbances and $n = 1, 2...$ is the stage of oscillation. The parameter n represents the number of vortices which travel simultaneously downstream across the opening. Validation of equation (1) is provided by phase measurements[29] of velocity fluctuations at upstream and downstream edges : a phase difference that is approximately an integer multiple of 2π can be observed.

First models for the prediction of tone frequencies[2,27] are based on the empirical hypothesis of $n2\pi$ phase criterion. Those models do not highlight the physical mechanism that leads to the periodic organization of the grazing flow. In fact, a simple analytical description of the different complex phenomena - non-linear instability growth, flow-trailing edge interaction, disturbance conversion near flow separation... - that are involved in sheartone is very difficult. However, a simplified linear approach, such as proposed by Howe,[11,12] can yield an insight into the feedback process. In his work, the shear layer is modeled by an infinitesimally thin vortex sheet. Thus, linear instabilities can be expressed in term of transverse displacement of the sheet. Under the hypothesis of very low Mach number, he shows that a criterion for self-sustained oscillations can be obtain by imposing the Kutta condition at the leading edge of the opening. Oscillations occur when the total unsteady flow generated by the naturally unstable shear layer ensures the tangential separation of the flow at the upstream edge. Even if this simplified theory provides a parametric evaluation of the possible self-sustained oscillation ranges, some physical aspects should be added in the model to obtain an indication of the preferred stage of oscillation. Indeed, the source terms of the linear vortex sheet approach are only modeled by the energy exchange between mean flow and crosswise transient velocity. The streamwise fluctuations and the contribution of mean velocity gradient are completely neglected. Moreover, Howe's model assumes that the shear layer has a negligible thickness. Then, the mathematical representation of instability waves does not include the complex evolution of the wave number and spatial growth rate of instability as a function of the shear layer thickness.[17]

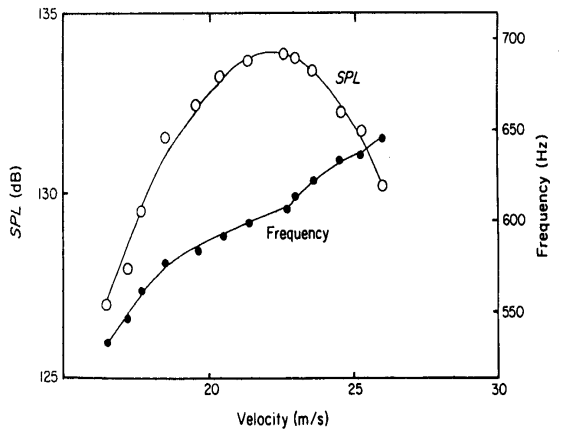

Figure 2: Frequency response of a Helmholtz-like cavity under aerodynamic excitation as function of flow velocity (Nelson *et al.*[18]). • : frequency; ○ : Sound Pressure Level.

Hence, the restrictive simplifications do not allow a trustingly prediction of the true unstable range of successive discrete tones, which can be observed for example in the experimental work (see figure 1) performed by Ziada and Rockwell[29,30] on a mixing-layer-wedge arrangement in a water tunnel. The first four stages of oscillation, separated by frequency jump, can be discerned. This experimental result shows that the frequency of oscillation has to be in the neighbourhood of the frequency β_{max} at which the shear layer is the most unstable. A value of this frequency β_{max} can be provided by the inviscid linear stability theory.[17] Ziada and Rockwell have also calculated the theoretical evolution (dashed curves) of the sheartone frequencies for each stage using equation (1). The convection velocity U_c depends on the upstream velocity U_0, the characteristic momentum thickness θ_m and the aerodynamic wave length. The characteristic momentum thickness of the shear layer θ_m is taken at the distance $x_m = 10\ \theta_0$ from the leading edge.[30] This experimental investigation has been used in this work as a benchmark case for numerical simulations (part 3).

1.2 Frequency matching and acoustic coupling

If the sheartone is generated over the mouth of a cavity resonator such as the passenger compartment in case of sunroof buffeting problem, a maximum acoustic level will be observed inside the cavity when resonance frequency and sheartone frequency are equal. For a given operating stage, the sheartone frequency (1) varies nearly linearly with the flow velocity. Thus, a critical speed range for which the sheartone frequency is close to the Helmholtz frequency of the vehicle may exist. Experimental investigations[3,7,18] indicate that, at frequency matching, there is a strong increase of the amplitude of aerodynamic fluctuations. The acoustic flow at the orifice greatly enhances the growth rates of the instability waves. Then, the assumption of linear development of oscillating waves is no longer valid and it appears that non-linear effects induce a concentration of the vorticity shed at the upstream edge into coherent vortices. Moreover, frequency variation plotted as a function of the grazing flow velocity in figure 2 shows a frequency lock-on of the vortex shedding around the resonance frequency ($f_{exp} \approx 600$ Hz) of the cavity : the transverse acoustic velocity triggers the shedding of new disturbance. The strong phase coupling between vortical and acoustic fluxes can be observed by flow visualization.[3,18] A vortex is shed from the leading edge at the moment at which the pressure inside the cavity reaches a minimum. This experimental result is frequently used in non-linear models[14,3,13] that predict oscillation frequency for acoustic coupling conditions. But the linear theory[12,15] in presence of transverse unsteady flow (the acoustic flow) shows that this phase relation can be also found by the application of the Kutta condition at the leading edge. The idea of the control of vortex generation by the Kutta condition was intuited by Nelson *et al.*[19] : at each period the vortex produced induces a velocity at the upstream edge which exactly cancels the acoustic potential flow. Furthermore, Kutta condition implies naturally that the amplitude of acoustic flow controls vorticity concentration, which fixes in turn the amplitude of the reciprocal aerodynamic velocity.

Thus, it is worth noting that both for off-resonant conditions, i.e. when the sheartone feedback mechanism is predominant, and for acoustic-flow coupling, the coherent and periodic organization of aerodynamic disturbances arises from the same physical constraint.

Most of flow-excited cavity models at low Mach number are based on the acoustic coupling assumption.[3,7,13,14] Hence, the aerodynamic feedback loop described previously is not taken into account. This simplification has little importance near critical flow speeds because both phase and amplitude of vortices are imposed by the acoustic flux. Then, it is not surprising that predictions of oscillation frequencies compare favorably with experiments. Nevertheless,

if the flow speed is moved away from the frequency matching domain, the sheartone mechanism is no more negligible and self-sustained oscillations can persist. Consequently, those models do not provide a good prediction of the onset and termination velocity of the oscillations : the critical speed range of flow buffeting is systematically underestimated.[13,14]

The physical investigation of the self-excited flow oscillations points up all the mechanisms that we need to compute for the simulation of the whole of sunroof buffeting phenomenon. Since the successful excitation of the Helmholtz resonance is usually dependent on the possibility of advantageous cooperation with a suitable sheartone, it is necessary to compute simultaneously the two oscillation processes. A commercial CFD solver is used in this study. The aim of this work is to study the ability of this solver to simulate all the basic physical phenomena involved in the sunroof buffeting. A general presentation of the numerical method and an aerodynamic validation of the solver are presented in Part 2. The suitability of the code to predict sheartone mechanism is discussed in Part 3. Acoustic simulations, with no-flow conditions, are reported in Part 4. Finally, a Helmholtz-like flow-excited cavity has been computed (Part 5). Numerical results are compared to experimental data extracted from literature.

2. Presentation of Lattice Boltzmann simulations

The CFD code PowerFLOW is used to compute unsteady flow physics. The basis of PowerFLOW is a lattice-based system built upon a mathematical approach called Lattice Boltzmann Method (LBM). Unlike conventional numerical codes which use a discretization of macroscopic continuum equations such as the Navier-Stokes equations, the LBM method is based on mesoscopic kinetic equations and a particle distribution function.

2.1 Lattice Boltzmann Method (LBM)

LBM is a discrete formulation of the Boltzmann kinetic theory. This theory describes the dynamical behavior of a gas with a continuum distribution function $f(\mathbf{x}, \mathbf{c}, t)$ which represents the number of particles whose positions and velocities are $\mathbf{x}$ and $\mathbf{c}$ at time t. Gas flows obey the Boltzmann equation

$$\frac{\partial f}{\partial t} + \mathbf{c} \cdot \nabla f = \Omega(f) \tag{2}$$

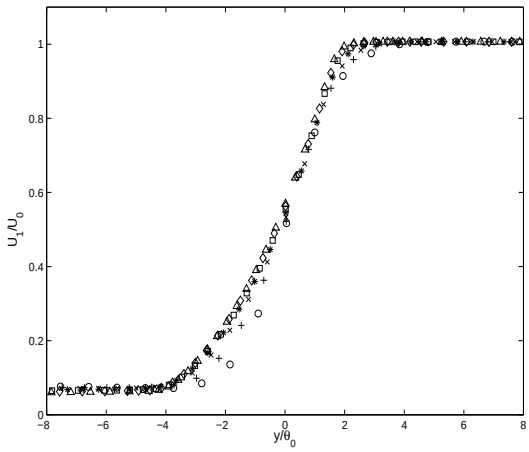

Figure 3: Free shear layer. Mean streamwise velocity at $\circ$: $x/\theta_0 = 26$; $+$: $x/\theta_0 = 53$; $\times$: $x/\theta_0 = 80$; $*$: $x/\theta_0 = 106$; $\square$: $x/\theta_0 = 133$; $\diamond$: $x/\theta_0 = 160$; $\triangle$: $x/\theta_0 = 186$.

where $\Omega(f)$ is a collision function which determines physics of the flow. The macroscopic variables such as density ρ, velocity $\mathbf{u}$ and internal energy ϵ are deduced from the first three velocity moments of the distribution function. Further details about this approach are given in Appendix A.

Because of the quadratic aspect of $\Omega(f)$ and the multiple integrations in its analytical formulation, different simpler models have been introduced. The most straightforward choice of collision operator is the linearized collision operator with a single relaxation time τ or the Bhatnagar-Gross-Krook (BGK) approximation[21]

$$\Omega = -\frac{f - f^{(eq)}}{\tau} \tag{3}$$

where $f^{(eq)}$ is the equilibrium function. The discretization process of the Boltzmann equation (2) is similar to that introduced for the discretization of kinetic equation in the Lattice Gas Automata.[9] Other information about equilibrium function and numerical formulation used in the PowerFLOW solver can be found in Appendix B.

2.2 Turbulence modeling

The fluid behavior in PowerFLOW lattice Boltzmann model obeys the Navier-Stokes equations for hydrodynamic length scale $L_h \geq \Delta x / (\omega_c \Delta t)$ where Δx and Δt are the spatial and time steps, and ω_c a relaxation parameter (see Appendix B). Hence, in most cases, L_h is greater than Kolmogorov length

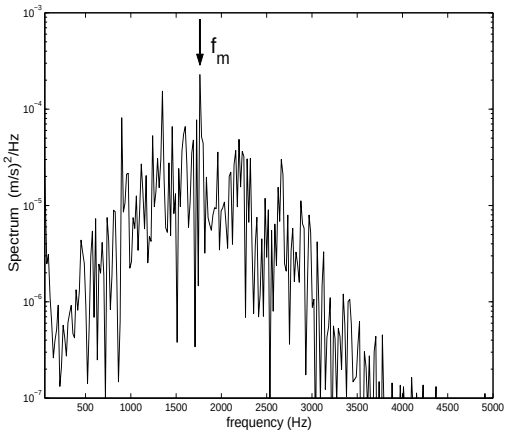

Figure 4: Spectrum of the transverse velocity at $x/\theta_0 = 150$, $y = 0$. Frequency resolution $\Delta f = 18$ Hz.

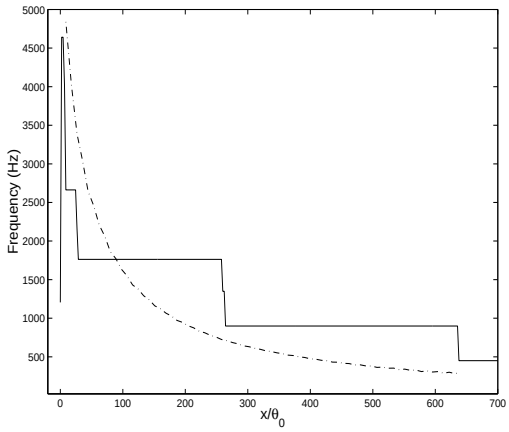

Figure 5: Frequency of the maximum amplitude component at the centreline. ——— LBM simulation; – · – · linear theory. Frequency resolution $\Delta f = 18$ Hz.

scale of the flow. A modeling of the effects of subgrid turbulent fluctuations needs to be introduced. A turbulent viscosity and thermal conductivity are added to the resolved flow quantities. The turbulent viscosity has the classical form $\nu_T \propto k\tau$, where k is the kinetic energy and τ accounts for non-equilibrium time scales such as that induced by the mean rate of turbulent dissipation ϵ. Calculation of ν_T involves two additional equations for k and ϵ based on the Renormalisation Group model.[28] Those equations are solved on the same lattice with a Lax-Wendroff second-order finite-difference scheme. Furthermore, an extended wall law that accounts for pressure gradient effects is used.[28]

2.3 The bidimensional free mixing layer

The present benchmark case has been chosen in order to study the possibility of performing turbulent simulations with the solver. A free shear layer expands from a splitter plate of height h between two parallel flows. The characteristic Reynolds number is $Re_{\theta_0} = \Delta U \theta_0/\nu = 110$ with $\Delta U = 18$ m/s. The thickness ratio between the initial flow and the splitter plate is $h/\theta_0 = 4.3$. This case corresponds exactly to the configuration simulated in the next part without the impingement wedge (see figure 6). PowerFLOW uses a structured, cubic Cartesian mesh and a grid refinement scheme which refines the grid size in each direction equally and successively by a factor two.[8] The minimum grid size is $\Delta x_{min} = 10^{-4}$ m which leads to $y^+ \approx 16$ on the upper side of the splitter plate, near the separation edge. Eight levels of grid resolution are used. The time step is tuned in each resolution regions to ensure a constant CFL = 0.79.

The mean feature of the turbulent shear layer is the self-similarity of mean profiles that implies a linear growth of the momentum thickness θ with the streamwise distance x. Figure 3 presents mean velocity profile in dimensionless form. In the range of plotted streamwise location, the self-similarity of the flow is well reproduced. The growth rate of the shear layer is $\partial\theta/\partial x \approx 0.035$. This value is in good agreement with that obtained for example by Rogers and Moser.[24]

The LBM time-dependent calculation handles the development of large-scale structures in the shear flow. As shown in figure 4, the spectrum of the velocity fluctuations peaks at frequencies corresponding to the convection of large-scale instabilities. The linear theory[17] is a relevant method to get an estimate of the expected location of the main spectrum peak. The numerical and theoretical frequency of the peak f_m is plotted as function of the streamwise distance in figure 5. The step-like evolution of the frequency is due to the fact that only the largest flow structures are computed, then the unsteady development of the shear layer is only supported by vortex pairing. This behavior was already observed in a previous unsteady Reynolds-averaged Navier-Stokes (URANS) equations simulation of a plane mixing layer.[1] Nevertheless, at each streamwise location, the frequency of the coherent structure is close to the theoretical value.

Further analyses of velocity signals show that the

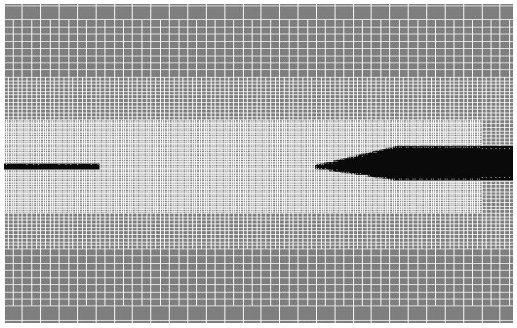

Figure 6: Zoom on the system : splitter plate (on the left) and impingement wedge (on the right). The fastest flow is in the upper region. Cubic cell grid with the last four refinement regions is also represented.

amplitude of aerodynamic disturbances is too weak compared to experimental data.[20] This default is due to the damping effect of the eddy viscosity model based on the $k-\epsilon$ RNG equations. However, the low dissipative nature of the numerical process allows to compute naturally growing instabilities in the shear flow. This weak numerical dissipation is one of the advantages of LBM in comparison with traditional CFD methods based on the discretization of Navier-Stokes equations.

3. Aerodynamic feedback : simulation of the sheartone

Experiments of Ziada and Rockwell[29,30] have been chosen for simulations of the sheartone. An impingement wedge is placed at a variable distance L downstream the leading edge. Geometry of the system is shown in figure 6. The characteristic Reynolds number based on the distance between the leading edge and the impingement wedge is $Re_L = \Delta U L/\nu = 11300$ with $\Delta U = 18$ m/s. As pointed out in part 1.1, the ratio L/θ_0 is a driving parameter that control the number of the sheartone stage. An initial value of this ratio is taken as $L/\theta_0 = 104$. The thickness of the incoming boundary layer is fixed by imposing its development length on the upstream no-slip wall. Before the limit of the boundary layer birth, a free-slip condition is applied on the solid wall.

Bidimensional turbulent calculations have been performed with different ratios L/θ_0 but flow velocity is held constant. Some snapshots of the vorticity field are shown in figure 7. For $L/\theta_0 = 104$, $L/\theta_0 = 294$ and $L/\theta_0 = 379$, stages 1, 2 and 3 of oscillation are successively obtained. The flow patterns compare well with flow visualizations of Ziada and Rockwell.[29] Other runs have been made for increasing impingement length L/θ_0 and the emergent frequency is plotted as a function of this ratio in figure 8. For each stage, the corresponding value of the parameter L/θ_0 differs from experimental measurements reported in figure 1 by a factor 5. Frequencies of successive sheartones lie around centered frequency $\beta_{sh} = f\theta_m/U_0 \approx 0.007$ which differs from the theoretical and experimental evaluation $\beta_{max} = 0.0167$. After more investigations, the frequency β_{sh} has been identified as a resonance frequency of the computational domain. The offset of L/θ_0 could be attributed to this shift of the preferred frequency of the shear layer. Despite of this numerical artefact, the mean features of sheartone phenomenon is well reproduced by the LBM method : an integer number of aerodynamic wavelengths in the opening for each stage, the decrease of oscillation frequency for a given stage and the jumps of frequency around a preferred value as L/θ_0 is increasing. In figure 8, we have also plotted theoretical curves given by equation (1) with the empirical value of the convection velocity $U_c = 0.5U_0$. We can see that evolution of computed frequencies shows good agreement with the simplified prediction formula. The fourth stage of oscillation observed in experi-

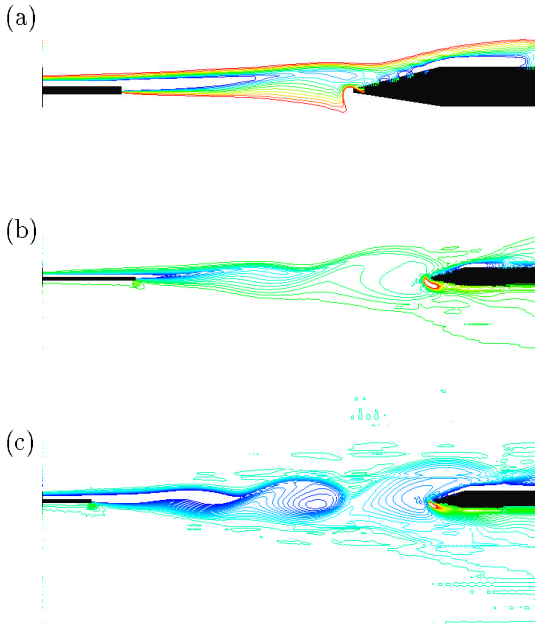

Figure 7: Isocontours of vorticity for the first three stages of oscillation. (a) : $L/\theta_0 = 104$, vorticity contours from -30000 s^{-1} to -10000 s^{-1}. (b) : $L/\theta_0 = 294$, vorticity contours from -35000 s^{-1} to 10000 s^{-1}. (c) : $L/\theta_0 = 379$, vorticity contours from -15000 s^{-1} to 33000 s^{-1}.

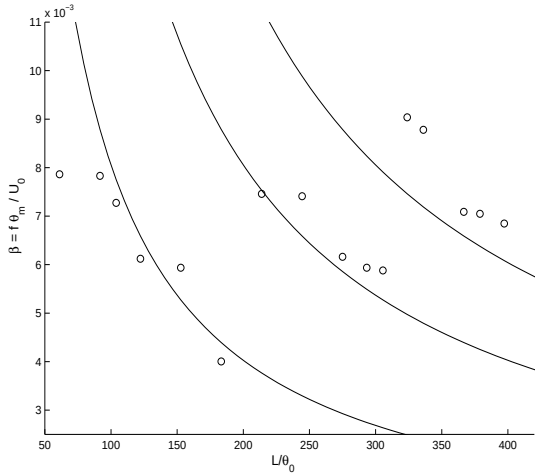

Figure 8: Calculated Strouhal number β of the shear layer oscillation as a function of impingement length L. ——— theoretical curves obtained with equation (1); ∘ : numerical results.

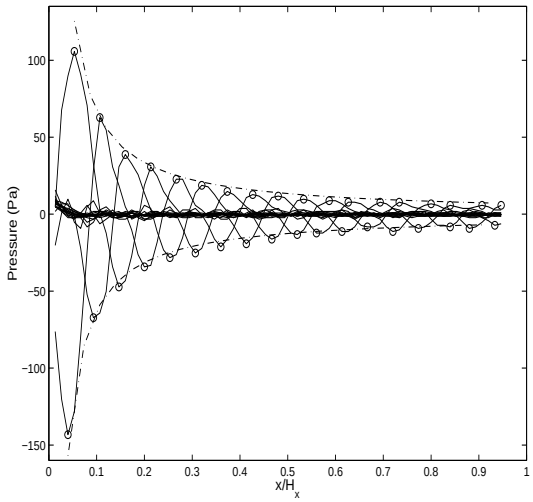

Figure 9: Amplitude decay of the positive and negative peaks. – · – · $1/r$ theoretical expression ; ∘ : calculated pressure peaks for successive times.

ments is not observed in our simulations. At this time, it is difficult to give an interpretation of this point.

4. Acoustic simulations

PowerFLOW describes a weakly compressible fluid with a self-consistently generated ideal gas equation of state. Thus, acoustics is a natural by-product of the flow simulation.

4.1 Acoustic pulse in a medium at rest

Initial spherical pressure pulse is imposed at the center of a tridimensional fluid space ($H_x = H_y = H_z = 3$ m). The grid size is uniform with $H_x/\Delta x = 150$. The radius of the source is $r_0 = 3\Delta x$. The initial overpressure condition leads to the propagation of positive and negative pressure peaks. We can consider that acoustic propagation is computed with around 6 points per wavelength. In this simulation, the turbulence model is used in order to keep the same numerical conditions for all the benchmark cases. In figure 9, numerical and theoretical amplitude decays of both peaks are represented along positive horizontal axis. The agreement between simulation and $1/r$ decay is very good. The suitability of BGK lattice Boltzmann model for sound wave propagation has been already shown in a recent work.[4] But we can note in figure 9 that background noise is quite important. Numerical high frequency oscillations can be also observed in pressure signals of figure 13. It is one of the current drawbacks of LBM which is a consequence of velocity discretization.

This simulation also provides information about how some boundary conditions handle the incidence of an acoustic wave. In the code, there is no specific boundary condition for the outgoing of acoustic waves. Then, *fixed static pressure* and *fixed velocity* with $U = 0$ are used on the boundaries of the fluid domain. In that run, reflection rate can not be evaluated precisely because of numerical background noise but it seems to be inferior to 15%. Thus, if we extend simulation domain far away from the source region, no spurious resonant modes will be expected to have a significant influence on the physical feedback mechanism of flow-excited cavity.

4.2 Acoustic response of a Helmholtz cavity

A Helmholtz-like cavity with baffled orifice is placed in the simulation domain. This cavity corresponds to a configuration studied by Nelson *et al.*[18,19] which will be used as a reference case for our flow-excited cavity computations (Part 5). The width and depth of the bidimensional cavity are $A = 0.058$ m and $D = 0.08$ m. The height and length of the resonator neck are respectively $h = 0.6$ mm and $L = 10$ mm. The length to depth ratio of the cavity is $L/D = 0.125$. The mesh grid and the numerical probes for pressure outputs are displayed in figure 10.

Acoustic response of the bidimensional cavity under a pulse excitation is calculated. The transfer

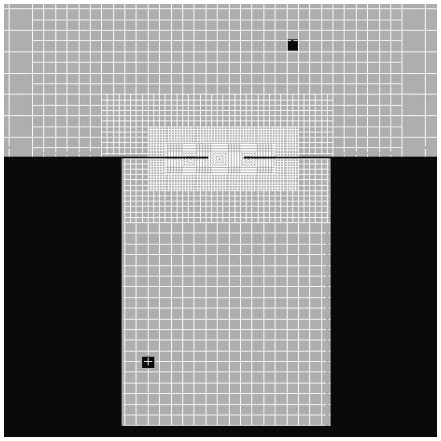

Figure 10: Simulated Helmholtz-like cavity. Refinement regions and numerical probes for pressure measurements are represented.

function between internal and external numerical probes is plotted in figure 11. Results are compared with an acoustic simulation performed with Boundary Element Method. The ability of the solver to simulate the resonant behavior of cavity is obvious. The first three acoustic modes can be observed in the plotted frequency range. The first peak at $f_r = 570$ Hz is the frequency of the Helmholtz resonance. The departure from the experimental value $f_{exp} \approx 600$ Hz is due to the bidimensional hypothesis of our simulation. It is worth noting that spatial discretization and boundary conditions used for this run are exactly similar to those used in the next part.

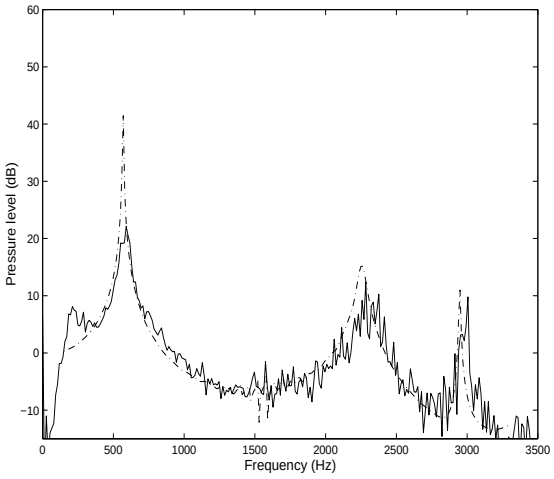

Figure 11: Spectrum of the transfer function between the two probes. ——— LBM simulation, frequency resolution $\Delta f = 13$ Hz ; – · – · BEM simulation, frequency resolution $\Delta f = 5$ Hz.

5. Simulation of a flow-excited cavity

The characteristic parameters of the simulation case are $Re_{\theta_0} = 78$ and $L/\theta_0 = 110$. Solid wall conditions were used to define the cavity mounted flushing the bottom limit of the simulation domain. The inflow boundary was treated using a constant velocity condition and fixed static pressure conditions were used for outflow boundaries (top and left sides of the domain). The minimum grid size is $L/(\Delta x)_{min} = 100$ in the resonator neck.

From simulation results reported in part 3 and 4, it is reasonable to expect that acoustic coupling phenomenon can be predicted by the solver. One way to confirm this acoustic coupling is to follow the frequency of oscillation during velocity increase. Frequency and amplitude curves of the pressure inside the cavity are plotted in figure 12 for inlet velocity varying from 6 m/s to 18 m/s. The frequency lock-on and the maximum amplitude of oscillations that we can see in figure 12 are typical consequences of acoustic coupling (see Part 1.2 and figure 2). Frequency at the critical velocity $U_{cr} = 13$ m/s is near the first resonance frequency of the cavity ($f_r = 570$ Hz) obtained in the previous part. As in experiments,[18] the flow buffeting results from the frequency matching between the first aerodynamic stage of oscillation and the Helmholtz resonance of the cavity. It must be noted that the value of 22 m/s for the critical velocity given in figure 2 by Nelson *et al*[18] was corrected to 12 m/s in the second companion paper.[19]

For the critical velocity, successive contours of vorticity (figure 13) show that the path of the vortex agrees with experimental observations of Nelson *et al*.[18] Indeed, with help of cavity pressure signal, we can see that the vortex is formed during the first half of cycle as the pressure in the cavity changed from its peak negative to its peak positive value ($0 < t < T/4$). During this period the acoustic transverse velocity is pointed inwards. The vortex reaches the mid-point of the orifice at the end of the first half cycle : at this stage, the flux of the resonator neck is at its maximum downward displacement ($T/4 < t < T/2$). During the next half cycle, the cavity pressure decreases and the airflow is displaced upwards ($T/2 < t < 3T/4$). On completion of the cycle, the vortex is almost ejected downstream the opening as the transverse flux reaches its maximum upwards displacement ($3T/4 < t < T$).

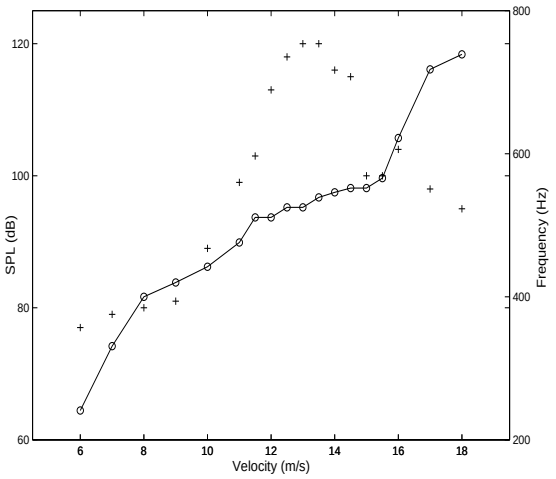

Figure 12: Frequency response of the cavity under flow excitation. ∘ : frequency; + : SPL.

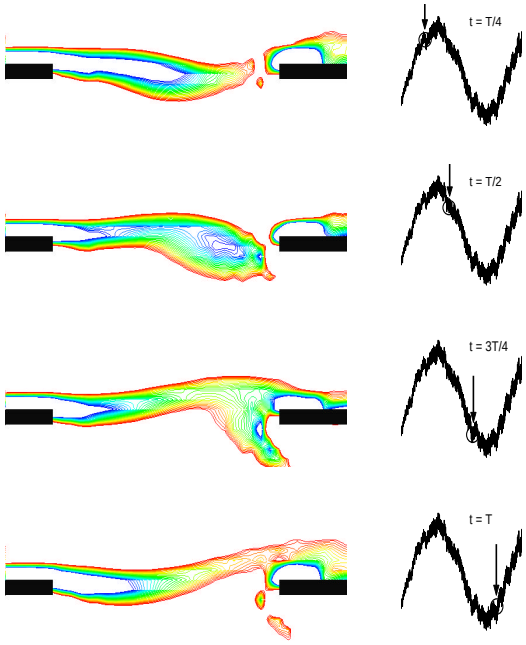

Figure 13: Isocontours of the vorticity field in the resonator neck for values between $-31240\ \mathrm{s}^{-1}$ and $-13600\ \mathrm{s}^{-1}$. On the right, pressure signal inside the cavity.

6. Concluding remarks

A short review of modeling and experimental investigations of cavity tone involving aerodynamic feedback and acoustic coupling has been proposed. Although numerous models for the shear layer-edge interaction and the mechanisms of feedback have been proposed, there is yet no generally accepted description of the details. However, some experimental observations and a simplified linear theory improve the comprehension of the phase-locking process.

For numerical approach, it has been shown that the main features of both aerodynamic and acoustic couplings can be predicted by PowerFLOW and those preliminary results are very encouraging for the simulation of sunroof buffeting. However, some problems have to be solved before obtaining an accurate prediction of the phenomenon. For example, we have seen that the ratio L/θ_0 is a fundamental parameter which selects the stage of oscillation of the sheartone. In our simulations, this parameter has to be shifted in order to recover the good stages of oscillation because the preferred oscillation frequency is not the expected frequency corresponding to the most-amplified disturbance of the shear layer. This problem seems to be linked with the dissipative effect of the eddy viscosity. Indeed, because of the overdamping of high frequency fluctuations, the preferred oscillation frequency is shifted toward a lower spurious resonance frequency of the computational domain. The turbulence modeling is still a limiting aspect of flow simulations with Lattice Boltzmann Method. Nevertheless, this new numerical method is less dissipative than classical URANS methods, particularly for acoustic waves. This is promising for future aeroacoustic applications at very low Mach numbers even if the residual background noise has to be reduced. For sunroof buffeting calculations, the numerical noise is not an important drawback because the pressure fluctuations inside the passenger compartment have very large amplitude. Moreover, the high levels of flow excitation by the acoustic flux allow to overcome the eddy viscosity damping. It is therefore possible to use the solver to study sunroof buffeting around the critical velocity. Of course, the accuracy of the evaluation of the buffeting velocity range will need to be discussed. However, it is already conceivable to use LBM for the design of wind deflectors.

Appendix A: From Boltzmann kinetic theory to Navier-Stokes equations

The general form of the Boltzmann kinetic equation is

$$\frac{\partial f}{\partial t} + \mathbf{c} \cdot \nabla f = \Omega\left(f\right) \tag{4}$$

Any solution of this equation requires an explicit expression for the collision operator $\Omega\left(f\right)$. However, several properties can be deduced without knowing the form of $\Omega\left(f\right)$.

The fluid density ρ, velocity $\mathbf{u}$ and internal energy e can be found from the distribution function as follows[6] :

$$\rho(\mathbf{x},t) = \int m f(\mathbf{x},\mathbf{c},t)\, d\mathbf{c} \tag{5}$$

$$\rho(\mathbf{x},t)\,\mathbf{u}(\mathbf{x},t) = \int m\mathbf{c} f(\mathbf{x},\mathbf{c},t)\, d\mathbf{c} \tag{6}$$

$$\rho(\mathbf{x},t)\, e(\mathbf{x},t) = \frac{1}{2}\int m|\mathbf{c}-\mathbf{u}|^2 f(\mathbf{x},\mathbf{c},t)\, d\mathbf{c} \tag{7}$$

where m is the molecular mass of the gas. For the collision operator $\Omega(f)$ to be mass, momentum and energy conservative, it is required that

$$\int \Psi_i \Omega(f)\, d\mathbf{c} = 0$$

for $\Psi_0 = 1, \Psi_1 = c_1, \Psi_2 = c_2, \Psi_3 = c_3, \Psi_4 = |\mathbf{c}|^2$, which are frequently called the elementary collision invariants. Hence, it is possible to derive all the continuum equations by multiplying Boltzmann's equation by Ψ_i, $i = 0, ..., 4$ and integrating over all velocities. Multiplying by m and using relations (5), (6) and (7), we obtain successively

$$\frac{\partial \rho}{\partial t} + \frac{\partial \rho u_i}{\partial x_i} = 0$$

$$\frac{\partial \rho u_j}{\partial t} + \frac{\partial\left(\rho u_i u_j + P_{ij}\right)}{\partial x_i} = 0$$

$$\frac{\partial\left[\rho\left(\frac{1}{2}u^2+e\right)\right]}{\partial t} + \frac{\partial\left[\rho u_i\left(\frac{1}{2}u^2+e\right) + P_{ij}u_j + q_i\right]}{\partial x_i} = 0$$

where P_{ij} is the total stress tensor and $\mathbf{q}$ is the heat flux which expressions depend on c_i and f . The five transport equations derived above from the Boltzmann equation are not the complete equations of hydrodynamics. There are always more unknown variables than equations. Then it is necessary to add some closure relations. Those relations can be found by performing a Chapman-Enskog expansion of the Boltzmann equation. Details of the Chapman-Enskog method can be found in reference [6].

As uniform classical gas relaxes to a Maxwellian distribution, the Maxwellian distribution emerges as an equilibrium solution of the Boltzmann equation. The collision operator $\Omega(f)$ in the Bhatnagar-Gross-Krook (BGK) approximation can take the form

$$\Omega(f) = -\frac{1}{\tau}\left(f - M[f]\right)$$

with

$$M[f] = \rho\left(\frac{m}{2\pi k_B T}\right)^{3/2} \exp\left[\frac{-m|\mathbf{c}-\mathbf{u}|^2}{2k_B T}\right] \tag{8}$$

where k_B is the Boltzmann constant. Navier-Stokes equations with some transport coefficients as viscosity ν and heat conductivity κ can be derived from Chapman-Enskog expansion of the BGK equation with the Maxwellian equilibrium function operator.

Appendix B: Lattice BGK model

In lattice Boltzmann model, the continuous distribution function is replaced by a discrete set of particle occupation numbers defined on a lattice of equal shaped cubic cells. This discretization is associated with a quantumisation of velocity vectors

$$\mathbf{c} \longrightarrow \{\mathbf{c}_i \;;\; i = 1, ..., p\}$$

$$f(\mathbf{x},\mathbf{c},t) \longrightarrow n_i(\mathbf{x},t)\,\Delta V$$

where ΔV is the unit cell volume. Spatial and time discretization is performed so that during an elementary time interval Δt particles can only hop from one center of a cell $\mathbf{x}$ to one of the p near neighbouring cells $\mathbf{x} + \mathbf{c}_i\Delta t$ according to their velocity $\mathbf{c}_i$. The lattice Boltzmann equation can be written as

$$n_i(\mathbf{x} + \mathbf{c}_i\Delta t,\; t + \Delta t) = n_i(\mathbf{x},\; t) + C_i(\mathbf{x},\; t)$$

In PowerFLOW solver the collision operator has the BGK approximation form

$$C_i(\mathbf{x},\; t) = -(\omega_c \Delta t)\left(n_i(\mathbf{x},\; t) - n_i^{(eq)}(\mathbf{x},\; t)\right)$$

where ω_c is a parameter called inverse collision time. The discrete Boltzmann BGK equation can be written as

$$n_i(\mathbf{x} + \mathbf{c}_i\Delta t,\; t + \Delta t) = (1 - \omega_c\Delta t)\, n_i(\mathbf{x},\; t) + \omega_c \Delta t\, n_i^{(eq)}(\mathbf{x},\; t)$$

Numerical process consists in calculating, at each $(\mathbf{x}, t)$, p algebraic relaxation-like equations. We see immediately that a great advantage of the method is the well-defined stability condition of the algorithm. At each cell and each time step, macroscopic fluid quantities are calculated using the discrete form of equations (5),(6) and (7). In PowerFLOW, the equilibrium function is assumed to have a polynomial form[21] which can be deduced from the expansion for small Mach numbers of the Maxwell equilibrium distribution function (8). A Chapman-Enskog expansion of the discrete BGK equation provides the three conservation equations for a viscous and heat conductive fluid that is supposed weakly compressible (Mach number < 0.3).

References

[1] Bastin, F., Lafon, P. & Candel, S., 1997. Computation of jet mixing noise due to coherent stuctures : the plane jet case. *J. Fluid Mech.*, **335**, 261-304.

[2] Bilanin, A.J. & Covert, E.E., 1973. Estimation of possible excitation frequencies for shallow rectangular cavities. *AIAA J.*, **11**(3), 347-351.

[3] Bruggeman, J.C., Hirschberg, A., Van Dongen, M.E.H. & Wijnands, A.P. 1991. Self-sustained aero-acoustic pulsations in gas transport systems : experimental study of the influence of closed side branches. *J. Sound Vib.*, **150**(3), 371-393.

[4] Buick, J.M., Greated, C.A. & Campbell, D.M., 1998. Lattice BGK simulation of sound waves. *Europhys. Lett.*, **43**(3), 235-240.

[5] Burroughs, C.B. & Stinebring, D.R., 1994. Cavity flow tones in water. *J. Acoust. Soc. Am.*, **95**(3), 1256-1263.

[6] Chapman, S. & Cowling, T.G., 1970. The mathematical theory of non-uniform gases. *Cambridge University Press.*

[7] Elder, S.A., Farabee, T.M. & DeMetz, F.C., 1982. Mechanisms of flow-excited cavity tones at low mach number. *J. Acoust. Soc. Am.*, **72**(2), 532-549.

[8] Exa Corp., 2000. PowerFLOW User's Guide 3.2. *Exa Corp.*, Lexington, MA.

[9] Frisch, U., Hasslacher, B. & Pomeau, Y., 1986. Lattice-Gas Automata for the Navier-Stokes equation. *Phys. Rev. Lett.*, **56**(14), 1505-1508.

[10] Hardin, J.C. & Pope, D.S., 1995. Sound generation by flow over a two-dimensional cavity. *AIAA J.*, **33**(3), 407-412.

[11] Howe, M.S., 1981. On the theory of unsteady flow over a slot. *Phil. Trans. R. Soc. Lond.*, **A 303**, 151-180.

[12] Howe, M.S., 1997. Edge, cavity, and aperture tones at very low mach numbers. *J. Fluid Mech.*, **330**, 61-84.

[13] Kook, H., Mongeau, L., Brown, D.V. & Zorea, S.I., 1997. Analysis of interior pressure oscillations induced by flow over vehicle openings. *Noise Control Eng. J.*, **45**(6), 223-234.

[14] Mast, T.D. & Pierce, A.D., 1995. Describing-function theory for flow excitation of resonators. *J. Acoust. Soc. Am.*, **97**(1), 163-172.

[15] Meissner, M., 1992. Discrete sound induced by low mach number flow over side branch deep cavity in a rectangular duct. *Archives of Acoustics*, **17**(2), 287-305.

[16] Meissner, M., 1993. Experimental investigation of discrete sound production in deep cavity exposed to airflow. *Archives of Acoustics*, **18**(1), 131-156.

[17] Michalke, A., 1965. On spatially growing disturbances in an inviscid shear layer. *J. Fluid Mech.*, **23**(3), 521-544.

[18] Nelson, P.A., Halliwell, N.A. & Doak, P.E., 1981. Fluid dynamics of flow excited resonance, part I : experiment. *J. Sound Vib.*, **78**(1), 15-38.

[19] Nelson, P.A., Halliwell, N.A. & Doak, P.E., 1983. Fluid dynamics of flow excited resonance, part II : flow acoustic interaction. *J. Sound Vib.*, **91**(3), 375-402.

[20] Oakley, T.R., Loth, E. & Adrian, R.J., 1996. Cinematic particle image velocimetry of high-Reynolds-number turbulent free shear layer. *AIAA J.*, **34**(2), 299-308.

[21] Qian, Y.H., D'Humières, D. & Lallemand, P., 1992. Lattice BGK models for Navier-Stokes equation. *Europhys. Lett.*, **17**(6), 479-484.

[22] Ribaldone, E., Castelluccio, V. & Marchese, P., 2000. Experimental and numerical study of tonal noise in flow-excited cavities. *Proc. Seventh Int. Congress on Sound and Vib.*, 1323-1330.

[23] Rockwell, D., 1983. Oscillations of impinging shear layers. *AIAA J.*, **21**(5), 645-664.

[24] Rogers, M.M. & Moser, R.D., 1994. Direct simulation of a self-similar turbulent mixing layer. *Phys. Fluids*, **6**(2), 903-923.

[25] Rossiter, J.E., 1964. Wind tunnel experiments of the flow over rectangular cavities at subsonic and transonic speeds. *Aero. Res. Counc. R. & M.*, **3438**.

[26] Sarohia, V., 1977. Experimental investigation of oscillations in flows over shallow cavities. *AIAA J.*, **15**(7), 984-991.

[27] Tam, C.K.W. & Block, P.J.W., 1978. On the tones and pressure oscillations induced by flow over rectangular cavities. *J. Fluid Mech.*, **89**(2), 373-399.

[28] Teixeira, C.M., 1998. Incorporating turbulence models into the Lattice-Boltzmann Method. *Int. J. Modern Phys. C*, **9**(8), 1159-1175.

[29] Ziada, S. & Rockwell, D., 1982. Oscillations of an unstable mixing layer impinging upon an edge. *J. Fluid Mech.*, **124**, 307-334.

[30] Ziada, S. & Rockwell, D., 1982. Vortex-leading-edge interaction. *J. Fluid Mech.*, **118**, 79-107.